Supporting information

Encapsulated anion-dominated photocatalytic and adsorption performances for organic dyes degradation and oxoanion pollutants capture over cationic Cu(I)-organic framework semiconductors

Yan Zhao,[a, b] Lei Li,[a, b] Bo Ding,[b] Xiu-Guang Wang,[b] Zheng-Yu Liu,[b] En-Cui Yang,*[, b] Xiao-Jun Zhao*[, a, b]

[a] *Department of Chemistry, Collaborative Innovation Center of Chemical Science and Engineering, Nankai University, Tianjin 300071*, *People's Republic of China*

[b] *College of Chemistry*, *Key Laboratory of Inorganic-Organic Hybrid Functional Material Chemistry*, *Ministry of Education*, *Tianjin Key Laboratory of Structure and Performance for Functional Molecules*, *Tianjin Normal University*, *Tianjin 300387*, *People's Republic of China*

Physical measurements. Elemental analyses for C, H and N were carried out with a CE–440 (Leeman–Labs) analyzer. Fourier transform (FT) IR spectra (KBr pellets) were taken on an Avatar–370 (Nicolet) spectrometer in the range 4000–400 cm^{-1}. Thermogravimetric analysis (TGA) experiment was performed on a Shimadzu simultaneous DTG–60A compositional analysis instrument from room temperature to 800 ^oC under N_2 atmosphere at a heating rate of 5 ^oC min^{-1}. Powder X-ray diffraction (PXRD) patterns were obtained from a Bruker D8 ADVANCE diffractometer at 40 kV and 40 mA for Cu *K*α radiation (λ = 1.5406 Å), with a scan speed of 0.1 sec/step and a step size of 0.01^o in 2θ. The simulated PXRD pattern was calculated using single-crystal X-ray diffraction data and processed by the free Mercury v1.4 program provided by the Cambridge Crystallographic Data Center. UV–vis absorption spectra of photocatalytic and adsorption reaction were on a Shimadzu UV–2700 spectrophotometer in the range 200-800nm. UV/Vis diffuse reflectance spectra (DRS) were carried out on a U-4100 UV-vis spectrophotometer (HITACHI) equipped with an integrating sphere assembly. The scanning electron microscope (SEM) characterization and energy dispersive X–ray spectroscopy (EDX) analysis were performed by a field-emission scanning electron microscope (SEM, FEI NOVA Nano SEM 230) with energy dispersive X-ray spectroscope (EDX). Electrochemical Mott-Schottky plots were measured on an AMETEK Princeton Applied Research (Versa STAT 4) electrochemical workstation using MOF **1**/FTO or **2**/FTO combination as the working electrode, a platinum foil as the counter electrode and a saturated Ag/AgCl/KCl as the reference electrode. A 300 W Xenon lamp (CEL-HUV300) was used as the light source. The working electrode **1**/FTO or **2**/FTO were prepared by dropping 50 μL of sample suspensions containing photocatalyst **1** or **2** (3.0 mg), ethanol (1.0 mL), Nafion (20 μL) directly onto a FTO plate. The surface area of the working electrode exposed to the

electrolyte was about 0.64 cm^2. The Mott-Schottky plots of **1**/**2** electrode were measured in 0.2 M Na_2SO_4 aqueous solution (pH = 7). Electrochemical impedance spectroscopy (EIS) of **1** and **2** were carried out in 0.2 M Na_2SO_4 aqueous solution (pH = 7) with a bias of 2.0 V in the frequency range of 1−10 kHz. The photo-responsive signals of **1** and **2** were measured in 0.2 M Na_2SO_4 aqueous solution (pH = 7) under chopped light at 1.0 V.

Table S1 Selected bond lengths (Å) and angles (deg) for **1** and **2**.[a]

1		**2**	
Cu(1)–N(1)	2.018(5)	Cu(1)–N(1)	2.042(6)
Cu(1)–N(5)$^{\#2}$	1.985(5)	Cu(1)–N(5)$^{\#2}$	1.996(6)
Cu(1)–N(6)$^{\#1}$	1.979(5)	Cu(1)–N(6)$^{\#1}$	1.973(6)
N(6)$^{\#1}$–Cu(1)–N(1)	116.7(2)	N(6)$^{\#1}$–Cu(1)–N(1)	115.4(3)
N(6)$^{\#1}$–Cu(1)–N(5)$^{\#2}$	126.1(2)	N(6)$^{\#1}$–Cu(1)–N(5)$^{\#2}$	127.5(3)
N(5)$^{\#2}$–Cu(1)–N(1)	117.2(2)	N(5)$^{\#2}$–Cu(1)–N(1)	117.0(3)

[a] Symmetry codes for **1**: $^{\#1}$ $1-x, 1-y, z+1/2$, $^{\#2}$ $1/2+x, -1/2-y, z$. For **2**: $^{\#1}$ $1-x, 1-y, z-1/2$, $^{\#2}$ $1/2+x, -1/2-y, z$.

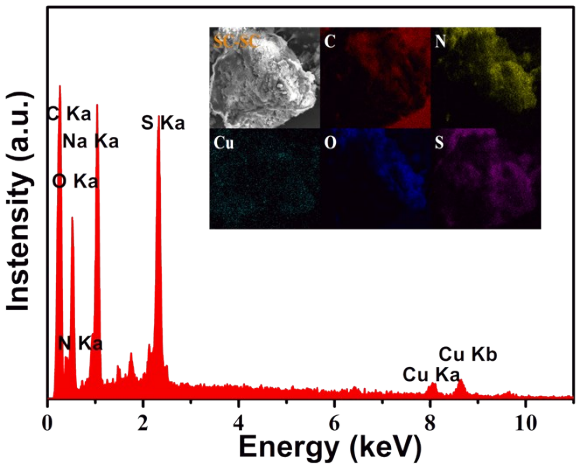

Fig. S1 EDX spectra and elemental mappings for **2** after being soaked into the saturated Na_2SO_4 solution.

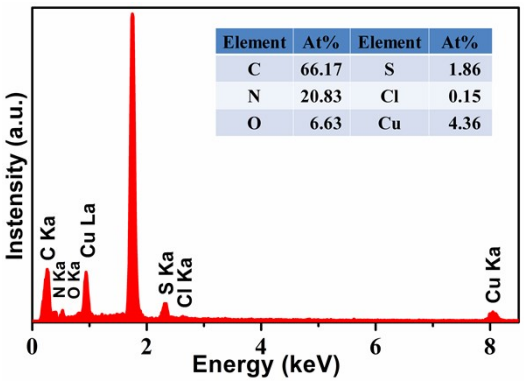

Fig. S2 EDX spectra and atomic ratio for **1** after being soaked into the saturated $Cu(ClO_4)_2$ solution.

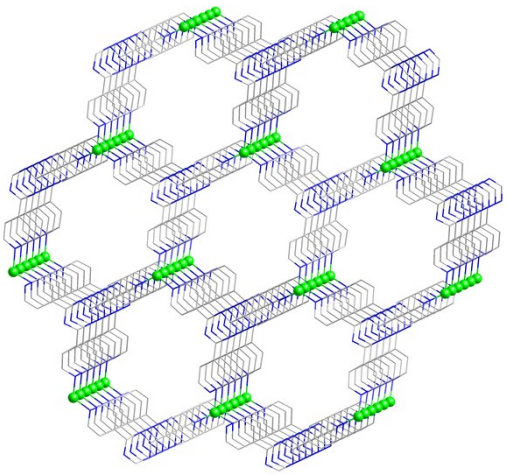

Fig. S3 Single (10,3)-*b* topology with **1**.

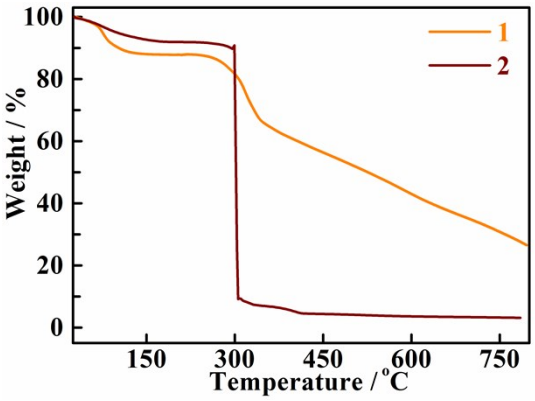

Fig. S4 TG curve for **1** and **2**.

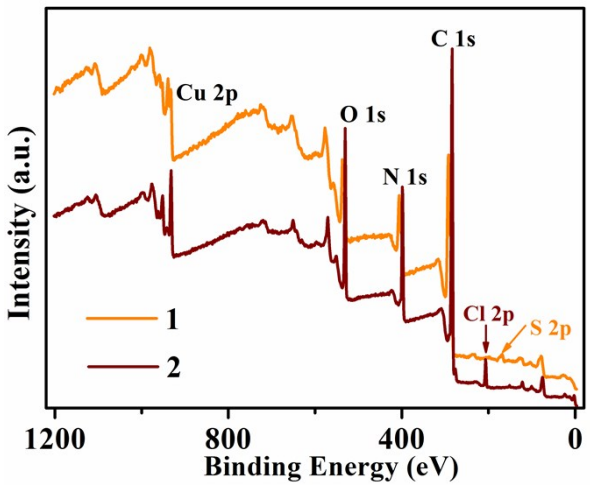

Fig. S5 Overall XPS spectra for **1** and **2**.

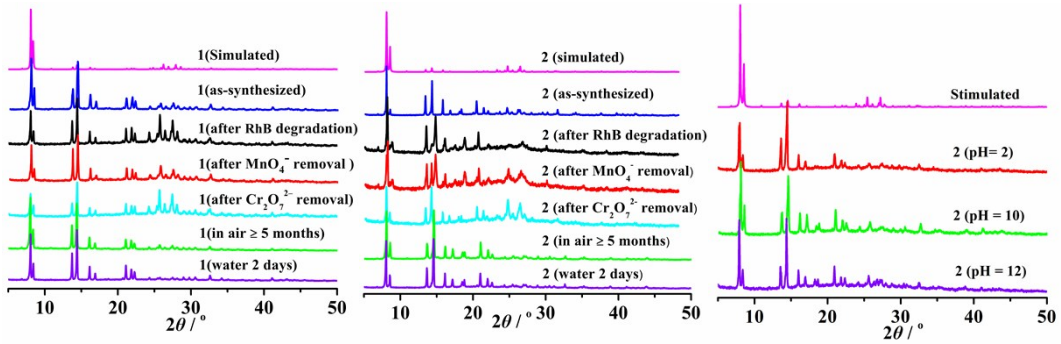

Fig. S6 Simulated and experimental PXRD patterns for **1** and **2**.

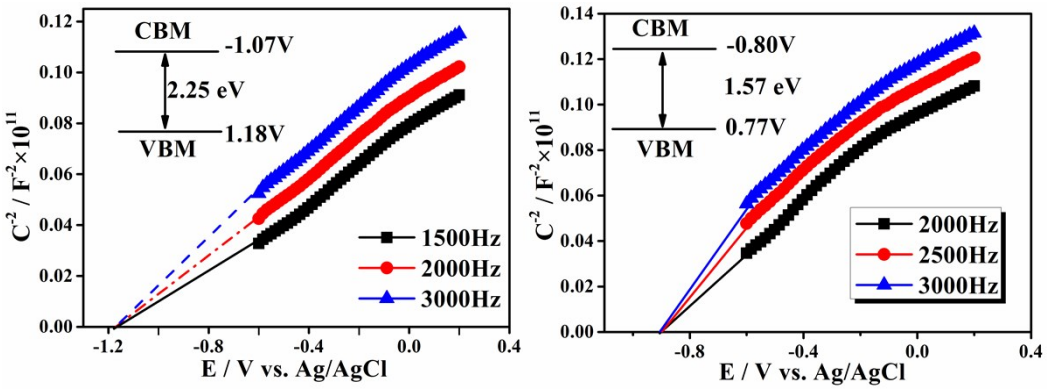

Fig. S7 Mott-Schottky curves of **1** and **2** measured in Na_2SO_4 aqueous solution.

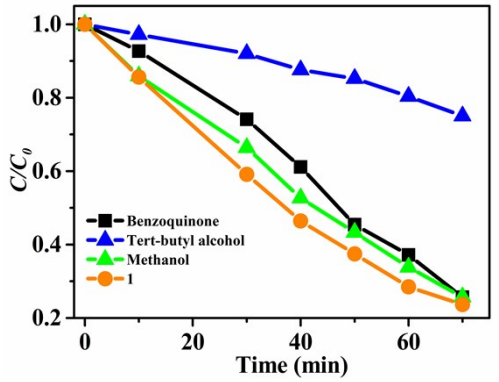

Fig. S8 Photodegradation efficiency over **1** in the presence of different free radical scavengers.

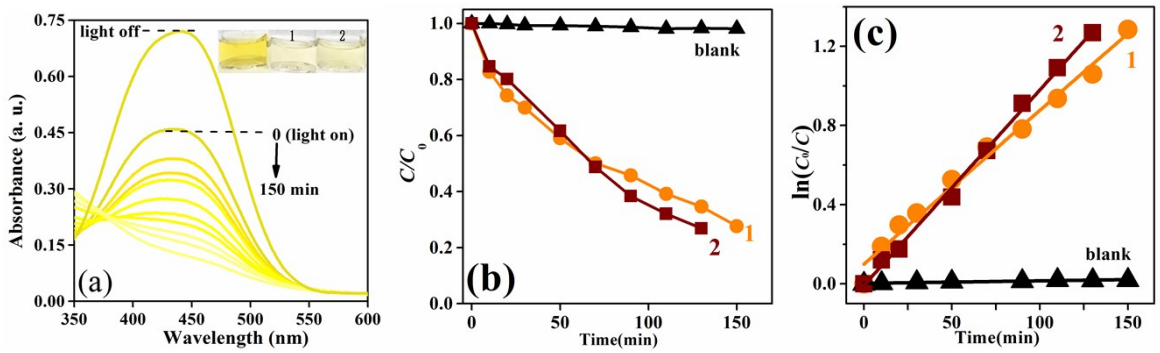

Fig. S9 (a) Time-dependent adsorption spectra of MY in the presence of **1** and H_2O_2 (Inset: photographs of aqueous My solutions before and after photodegradation). (b) C/C_0 of MY as a function of the irradiation time in the presence of H_2O_2, **1** and H_2O_2, as well as **2** and H_2O_2. (c) Plots of $\ln(C_0/C)$ vs. irradiation time for the photodegradation of MY over the photocatalysts.

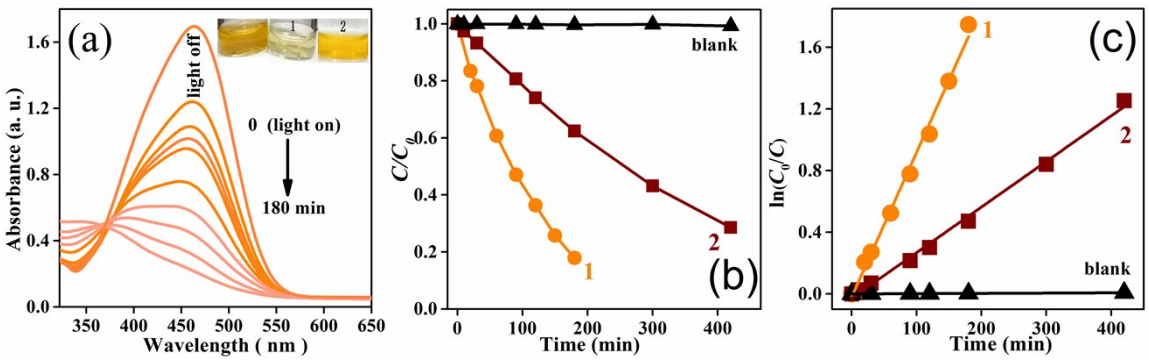

Fig. S10 (a) Time-dependent adsorption spectra of MO in the presence of **1** and H_2O_2 (Inset: photographs of aqueous MO solutions before and after photodegradation). (b) C/C_0 of MO as a function of the irradiation time in the presence of H_2O_2, **1** and H_2O_2, as well as **2** and H_2O_2. (c) Plots of $\ln(C_0/C)$ vs. irradiation time or the photodegradation of MO over the photocatalysts.

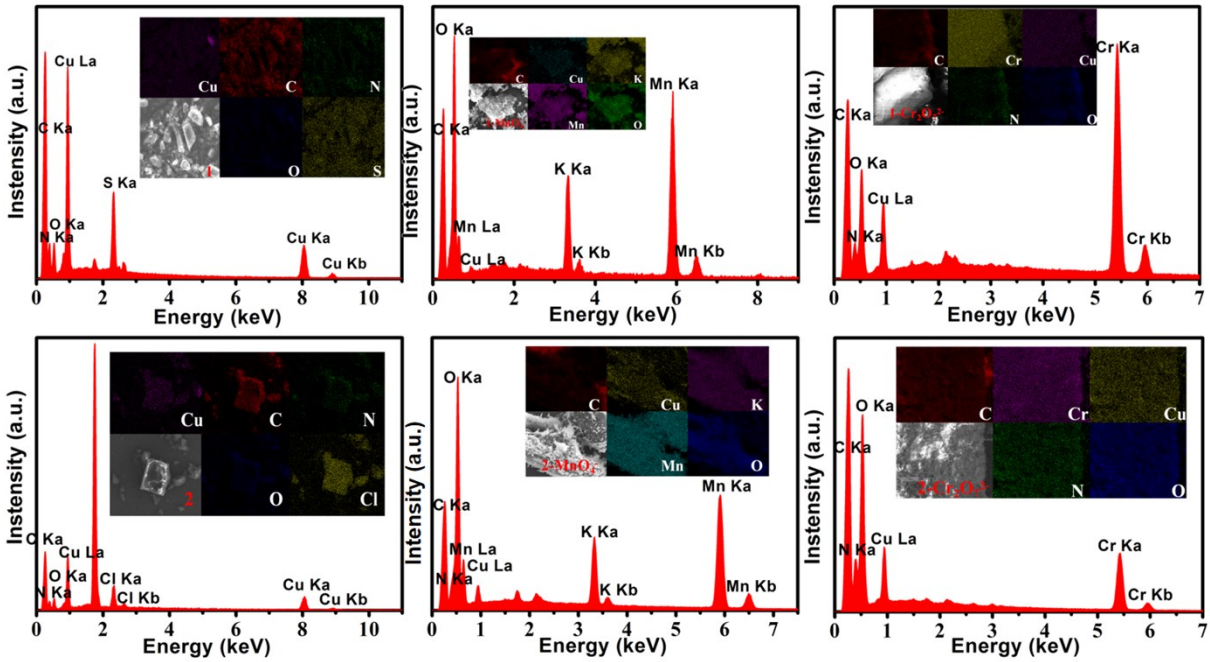

Fig. S11 EDX spectra and elemental mappings for **1** and **2** before and after adsorption of MnO_4^- and $Cr_2O_7^{2-}$ anions.

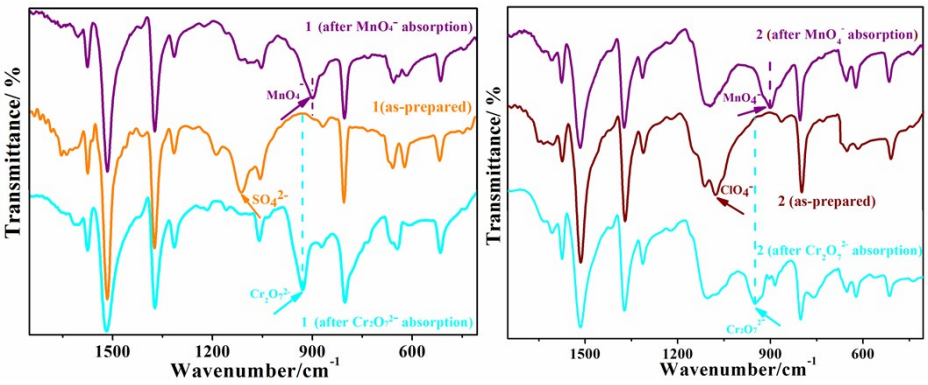

Fig. S12 FT-IR spectra of **1** and **2** before and after adsorption of MnO_4^- and $Cr_2O_7^{2-}$ anions.